



Available online at www.sciencedirect.com

jmr&t
Journal of Materials Research and Technology
www.jmrt.com.br



Original Article

Hybrid composites – a better choice for high wear resistant materials



Dora Siva Prasad^{a,*}, Chintada Shoba^b

^a Department of Mechanical Engineering, GITAM University, Visakhapatnam, India

^b Department of Industrial Engineering, GITAM University, Visakhapatnam, India

ARTICLE INFO

Article history:

Received 26 February 2014

Accepted 15 March 2014

Available online 6 April 2014

Keywords:

Hybrid composites

Rice husk ash

Wear

ABSTRACT

This investigation, studies the dry sliding wear behavior of aluminum (Al) matrix hybrid composites reinforced with rice husk ash (RHA) and silicon carbide (SiC) particulates up to 8% (in equal proportions) fabricated by vortex method. Pin-on disk wear test was carried out for both unreinforced alloy and hybrid composites. Scanning electron microscopy is used to study the wear characteristics of the unreinforced Al alloy and the hybrid composites. The results showed that the hybrid composites exhibits higher wear resistance than the unreinforced alloy. The wear mechanisms in the unreinforced alloy and the hybrid composites are analyzed and presented.

© 2014 Brazilian Metallurgical, Materials and Mining Association. Published by Elsevier

Editora Ltda. Este é um artigo Open Access sob a licença de [CC BY-NC-ND](http://creativecommons.org/licenses/by-nc-nd/4.0/)

1. Introduction

Metal matrix composites (MMCs) are becoming better substitutes for the conventional alloys because of characteristics like high stiffness, high strength and low density. Particulate reinforced aluminum alloy composites have shown a significant improvement in tribological properties including sliding and abrasive wear resistance [1–3]. Improvement in tribological properties of particle reinforced MMCs are due to the ceramic particle content, which protects the metal matrix from wear. One of the major problems with the aluminum alloys that limit their wear performance is their relatively poor seizure resistance in comparison to cast iron under dry sliding conditions [4]. Recently studies revealed that further improvements in the wear resistance of aluminum alloys can be achieved by incorporating two or more ceramic particles

[5,6]. Aluminum matrix composites with multiple reinforcements (hybrid composites) are finding increased applications because of improved mechanical and wear resistance and hence are better substitutes for single reinforced composites [7]. In an engine system the energy loss due to wear is about 41% as reported by Funatani and Kurosawa [8]. Al alloy/graphite particulate composite was used as a material for engine cylinders which exhibit higher seizure resistance and a lower frictional coefficient and wear rate compared with that of the aluminum reinforced with ceramic particulates [9–11]. RHA is an agricultural byproduct available abundantly in the world which contains above 90% of silica as a major constituent and the use of this silica rich RHA in the fabrication of composites would yield a low cost product with superior mechanical, wear and damping properties [12].

The present work was undertaken to manufacture A356.2 aluminum matrix composites reinforced with RHA and SiC

* Corresponding author.

E-mail: dorasivaprasad@gmail.com (D. Siva Prasad).

<http://dx.doi.org/10.1016/j.jmrt.2014.03.004>

2238-7854/© 2014 Brazilian Metallurgical, Materials and Mining Association. Published by Elsevier Editora Ltda.

Este é um artigo Open Access sob a licença de [CC BY-NC-ND](http://creativecommons.org/licenses/by-nc-nd/4.0/)

particles of different volume fractions using the vortex method. Microstructural characterization studies were carried out and finally, the wear mechanisms that are operative in the composites were investigated to aid in the correlation of the microstructure and properties of the composites.

2. Experimental

The composites were fabricated by using stir casting technique and the detailed experimental procedure is described in earlier works [2]. Composites containing 2, 4, 6, and 8 weight percentage RHA and SiC were fabricated. A standard Brinell hardness tester with 500 kg and 10 mm steel ball indenter was used to find the hardness of unreinforced alloy and hybrid composites. An average of five readings was taken of each sample for hardness measurements. Before conducting the wear tests the surface roughness of pins and the counter face steel disk were measured by using a Talysurf instrument (Model Surf Test SJ-301). The dry sliding wear tests were conducted on a pin-on-disk wear testing machine (Model: TL-20) according to the ASTM G99-04 standards. This machine is a versatile equipment designed to study wear under sliding condition only. The cylindrical pins of 8 mm diameter and 25 mm length were machined for conducting the wear experiments. Sliding generally occurs between a stationary pin and a rotating disk. The load is to be applied at the pin by dead weight arrangement. The system has a maximum loading capacity of 150 N. The cylindrical pins (8 mm diameter and 25 mm height) of the alloy/composite were used as test material. A steel disk was used as the counter face material. The wear tests were carried out at different loads of 9.81, 19.6, 29.41, 39.22 and 49.03 N. The sliding speed and sliding distance were maintained at 3.14 ms^{-1} (corresponding to disk speed of 600 rpm) and 3768 m, respectively for all the tests. The track radius was fixed at 50 mm. Wear tests were carried for 20 min. at room temperature without any lubrication. The photoelectric balance with an accuracy of $\pm 0.1 \text{ mg}$ was used to find the weight of the specimens before and after the experiments. The wear rate (W_r) is calculated using Eq. (1):

$$W_r = \frac{\Delta m}{L} \quad (1)$$

where Δm is the difference in mass before and after the wear experiment, and L is the sliding distance. The worn surfaces and worn debris of the unreinforced A356.2 alloy and hybrid composites were examined using scanning electron microscope (SEM) equipped with energy dispersive X-ray analysis (EDX).

3. Results and discussion

3.1. Microstructural characterization

Fig. 1 shows the scanning electron micrograph of the hybrid composite. It is observed that there is a uniform distribution of the reinforcement particulates in the alloy and no evidence of chemical reaction between the reinforcement and the matrix.

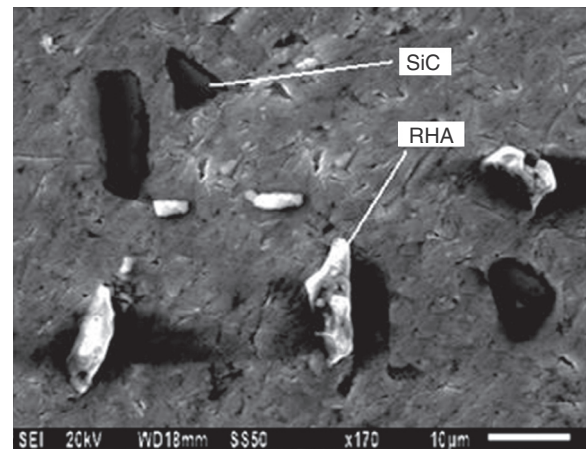


Fig. 1 – Scanning electron micrograph of the hybrid composite.

3.2. Hardness measurements

The hardness values of A356.2 alloy and the hybrid composites are given in **Table 1**. Apparently, the hardness of the composites is higher than that of A356.2 alloy and the hardness values of the composites increase with the increase of particle content. Increase in hardness results from the presence of relatively hard ceramic particulates in the matrix.

3.3. Surface roughness measurements

Surface roughness of pins and discs were found to be $R_a = 0.7 \mu\text{m}$ and $0.68 \mu\text{m}$, respectively. The roughness profile of the disk and the pins are shown in **Fig. 2a** and **b** respectively.

3.4. Wear of composites

The variation of weight loss and wear resistance (reciprocal of wear rate) as a function of normal load for the unreinforced alloy and hybrid composites was shown in **Figs. 3 and 4** respectively. It is seen from the plots that, with the addition of both reinforcement particulates, the wear rate of the composite is decreased. Also it could be seen that the wear rate (mass loss) increases as the normal load increases. The increase in the wear resistance can be attributed to the strengthening of the matrix due to the reinforcement, which results from an increase in the dislocation density as the percentage of reinforcement's increases.

Table 1 – Brinell hardness values of alloy and its composites.

S. no.	Sample	Hardness, BHN
1	A356.2 alloy	68
2	A356.2/2% RHA/2% SiC hybrid composite	74
3	A356.2/4% RHA/4% SiC hybrid composite	83
4	A356.2/6% RHA/6% SiC hybrid composite	96
5	A356.2/8% RHA/8% SiC hybrid composite	104

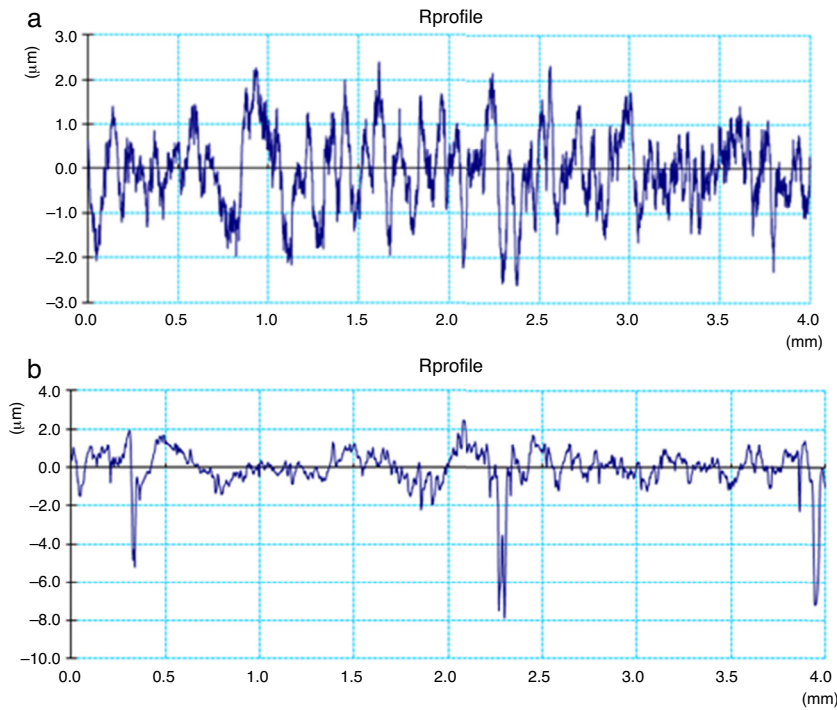


Fig. 2 – Roughness profile for (a) steel disk and (b) cylindrical pin.

Metal matrix composites are characterized by a large difference in the thermal expansion coefficient (CTE) of the matrix and the reinforcement (CTE of A356.2 is $21.4 \times 10^{-6}/^{\circ}\text{C}$, the CTE of RHA is $10.1 \times 10^{-6}/^{\circ}\text{C}$ and the CTE of SiC is $4.3 \times 10^{-6}/^{\circ}\text{C}$). Even small temperature changes, generate thermal stresses in the aluminum matrix. These stresses can be partially released by dislocation generation in the vicinity of the interface. Thus the dislocation density generated can be quite significant at the interface and can be predicted using the model of Taya and Arsenault [13] based on prismatic punching of dislocations

at a ceramic particulate. The dislocation density ρ at the interface is given by Eq. (2):

$$\rho = \frac{B\varepsilon V_r}{bd(1 - V_r)} \quad (2)$$

For hybrid composites Eq. (2) can be modified as

$$\rho = \frac{B\varepsilon(V_{\text{RHA}} + V_{\text{SiC}})}{bd\{1 - (V_{\text{RHA}} + V_{\text{SiC}})\}} \quad (3)$$

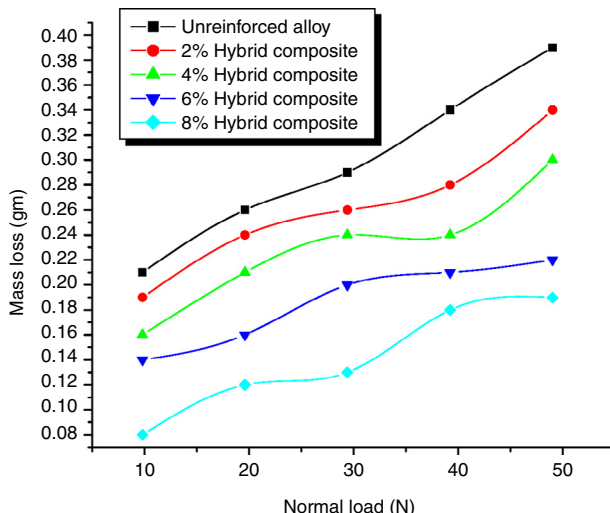


Fig. 3 – Variation of mass loss with % of reinforcement.

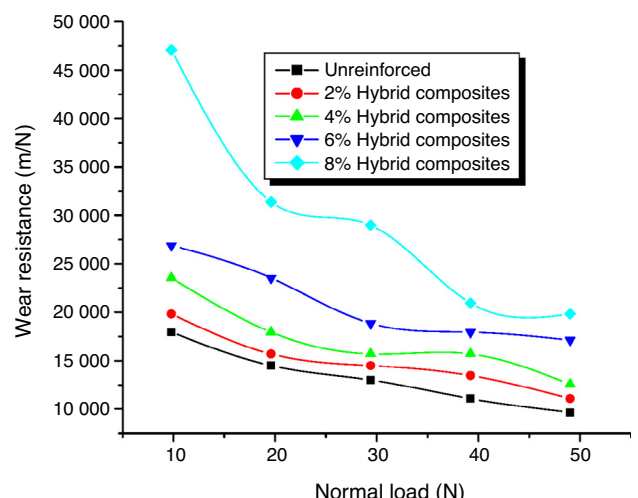


Fig. 4 – Variation of wear resistance with % of reinforcement.

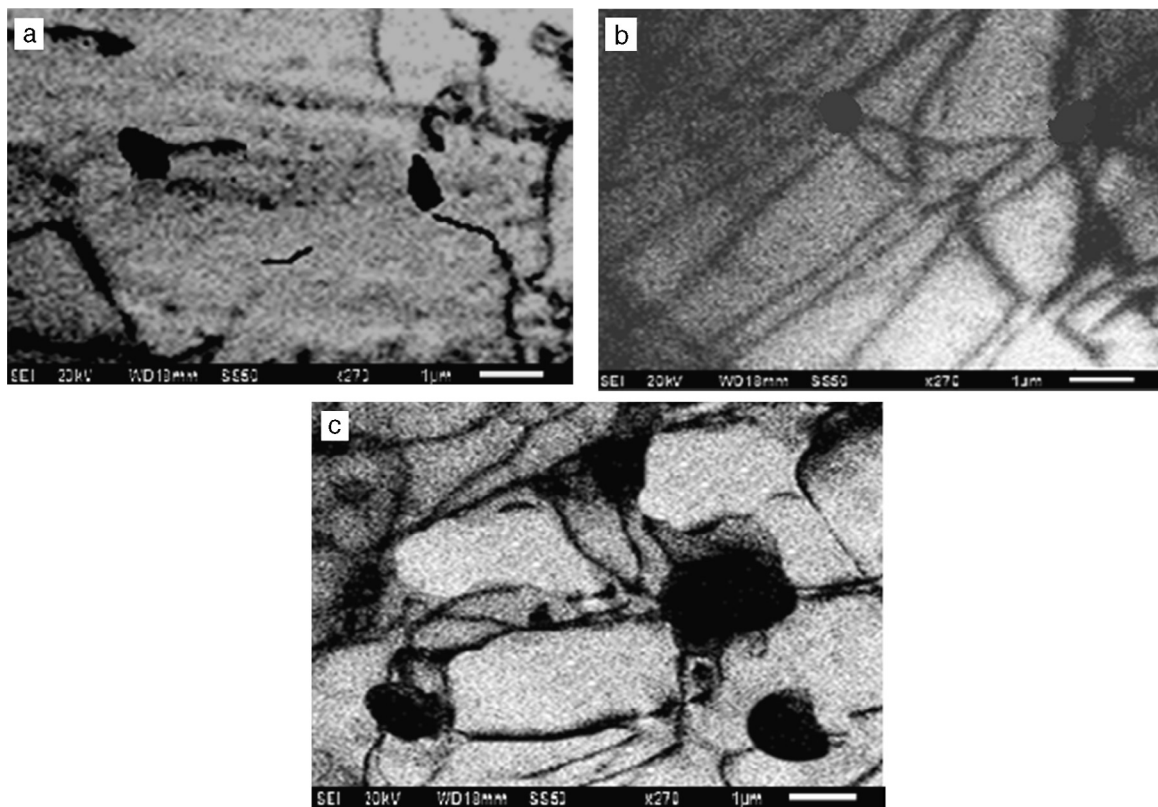


Fig. 5 – Scanning electron micrographs showing dislocation arrangement in (a) 4% hybrid composite, (b) 6% hybrid composite and (c) 8% hybrid composite.

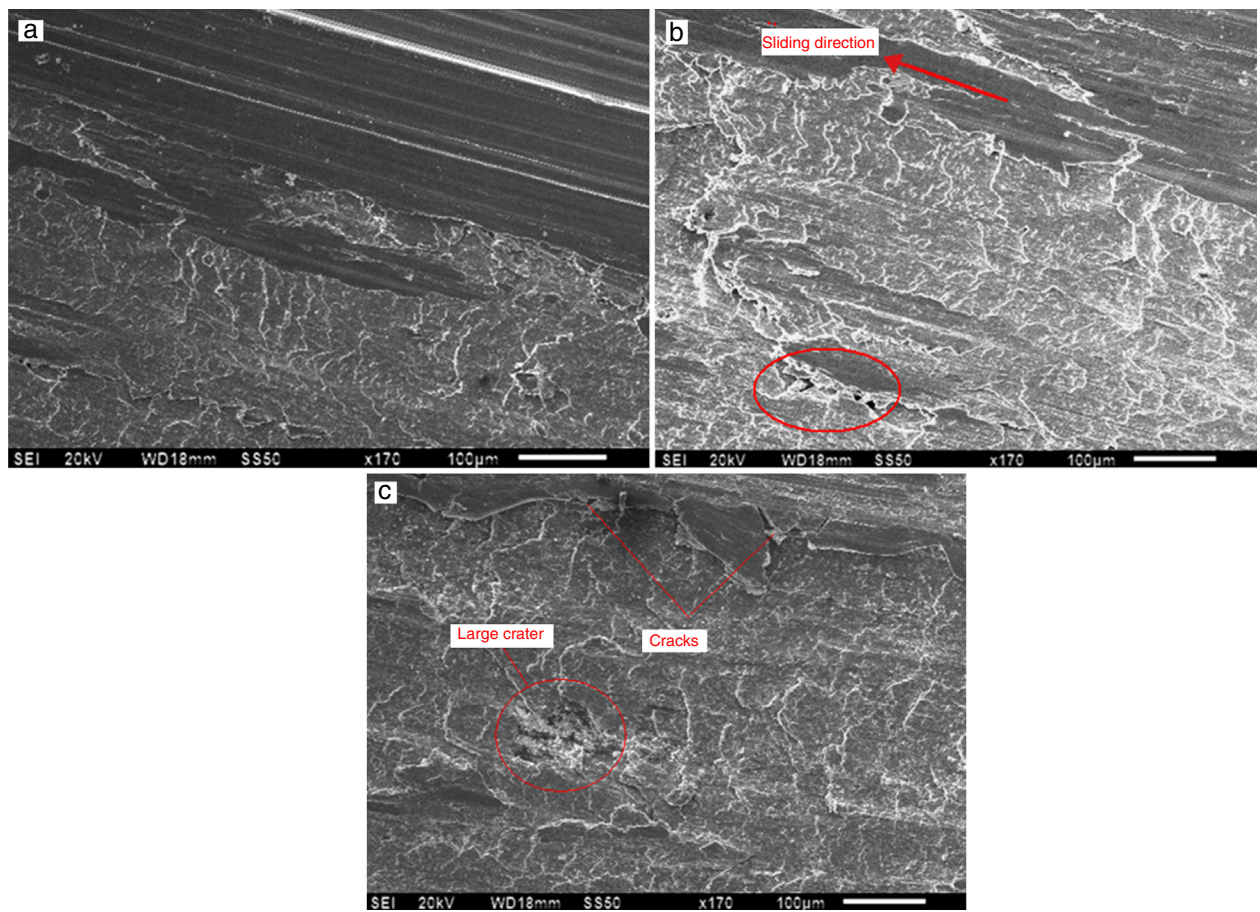


Fig. 6 – Morphologies of the worn surface of A356.2 alloy at a load of (a) 9.81 N, (b) 39.22 N and (c) 49.03 N.

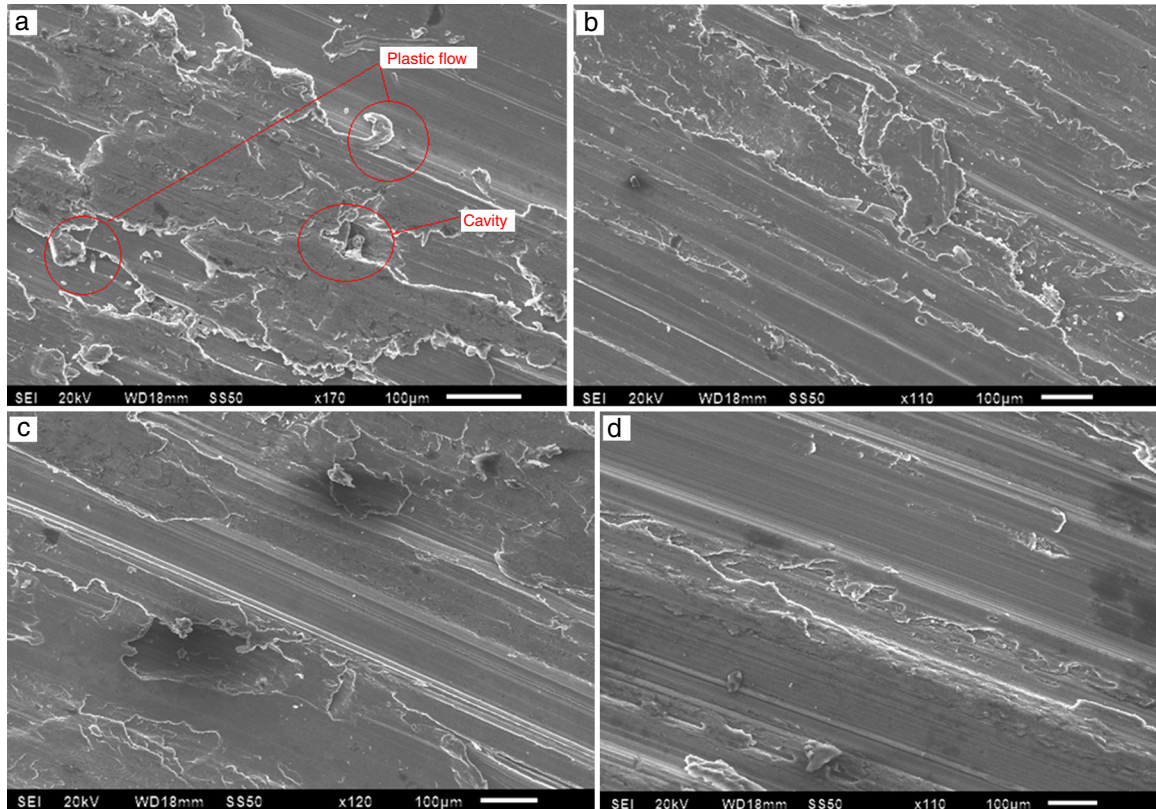


Fig. 7 – Morphologies of the worn surface at a load of 49.03 N (a) A356.2/2% RHA/2%SiC, (b) A356.2/4% RHA/4%SiC, (c) A356.2/6% RHA/6%SiC and (d) A356.2/8% RHA/8%SiC hybrid composite.

where B is a geometric constant that depends on the aspect ratio (it varies between 12 for equiaxed particulate and 4 for whisker-like particulate), ε is the thermal mismatch strain (the product of temperature change ΔT , during solidification of MMCs and CTE difference, $\Delta\alpha$, between reinforcement and matrix), V_r is the volume fraction of the reinforcement, b is the burgers vector, and d is the average grain diameter of reinforcements.

The strengthening due to the presence of dislocations generated by the difference in the CTE, the following equation may be used:

$$\Delta\sigma_T = \alpha G b (\rho)^{1/2} \quad (4)$$

where $\Delta\sigma_T$ is the yield strength contribution due to geometrical necessary dislocations, α is a constant (values 0.5–1), G is the shear modulus, and b is the Burger's vector. The dislocation density for the hybrid composites were then calculated based on Eq. (3). The detailed procedure was presented in earlier works [2] and the values are tabulated in Table 2. From Fig. 5a–c it is evident that there is an increase in the dislocations as the percentage of reinforcement increases.

3.5. Morphology of worn surfaces

Fig. 6a–c shows the worn-out surface of the base material at different loads of 9.81 N, 39.22 N and 49.03 N respectively. Fig. 6a shows the SEM micrograph of the worn-out surface of

Table 2 – Theoretical results of unreinforced and hybrid composites.

S. no.	Weight (%) of reinforcement	Estimated dislocation density, ρ (m^{-2})	CTE, α ($^{\circ}\text{C}$)
1	0.0	—	21.4×10^{-6}
2	2.0	17.31×10^{11}	17.44×10^{-6}
3	4.0	21.32×10^{11}	16.64×10^{-6}
4	6.0	23.99×10^{11}	16.09×10^{-6}
5	8.0	30.82×10^{11}	15.06×10^{-6}

the unreinforced alloy at a load of 9.81 N, from the micrograph it is observed that the worn-out surface consists of ridges and grooves running parallel to the sliding direction indicating abrasive wear and craters as evidences of adhesive wear. Fig. 6b shows the SEM micrograph of the worn-out surface of the base material at a load of 39.22 N. It was observed that the area of the craters increases indicating predominant wear in these areas. The SEM micrograph of the worn-out surface of the base material at higher load (49.03 N) is shown in Fig. 6c. From this micrograph it is observed a large cavity on the subsurface layer indicating severe loss of material. This feature is more significant as the load increases.

Fig. 7a–d shows the worn morphology of the hybrid composites at a higher load of 49.03 N. Fig. 7a shows the worn surface of A356.2/2%RHA/2%SiC hybrid composite. From the micrograph it is observed that there is plastic flow of the material along with small cavity in the subsurface layer with a little smooth patch indicating severe wear. The worn surface

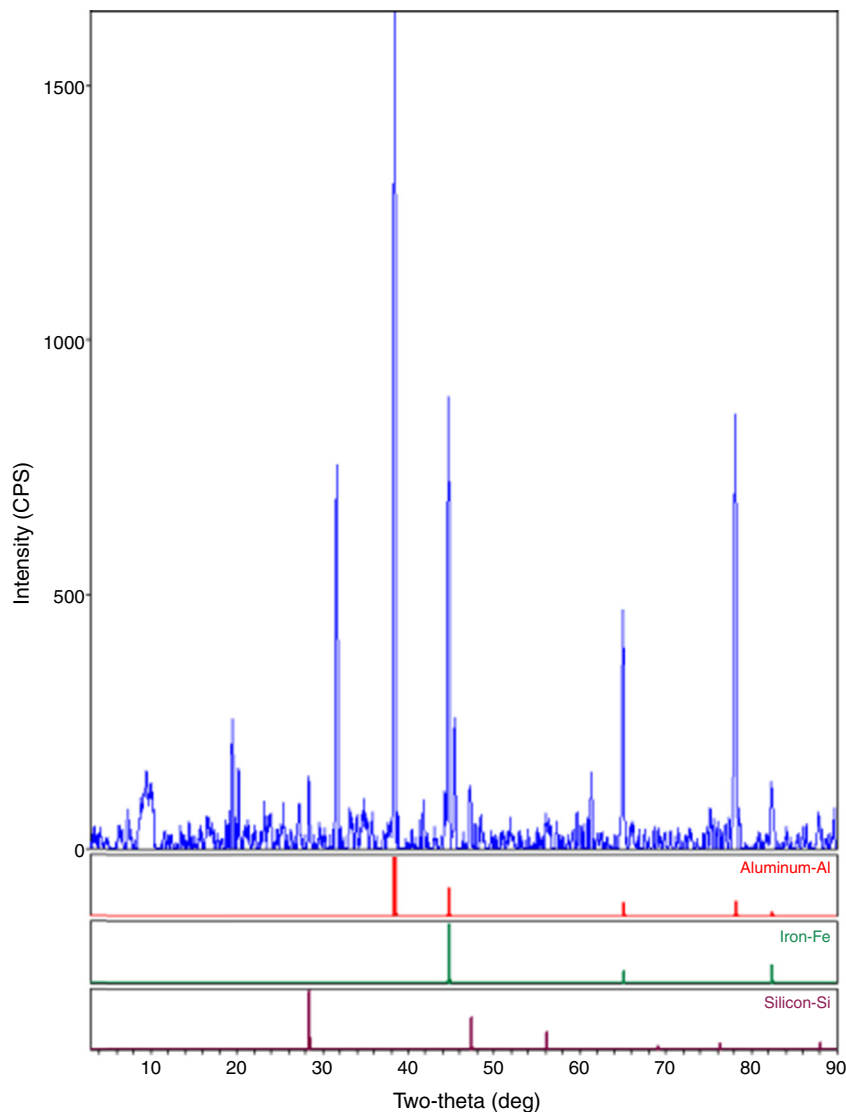


Fig. 8 – XRD pattern of 8% reinforced hybrid composite.

of A356.2/4%RHA/4%SiC hybrid composite is shown in Fig. 7b. It can be seen that there is a slight decrease in the plastic flow of the material and smooth patches and ridges are running parallel to the sliding direction indicating resistance to wear when compared to 2% reinforced and unreinforced alloy. As the percentage of reinforcement increase, these ridges and grooves become shallower and plastic flow zone of the material decreased indicating greater resistance to wear as shown in Fig. 7c and d. Also from Fig. 8 which represents the XRD pattern of the 8% reinforced composite sample. It is observed a peak corresponding to Fe, which indicates that mechanical mixing took place between the cylindrical pin and the counter face disk. This feature is more significant at higher loads rather than at lower loads.

4. Conclusions

From the present study, the following conclusions are drawn:

- The hardness of A356.2/RHA composites increased with the increasing weight percentage of rice husk ash content.
- The wear rate decreased with the increasing weight percentage of the RHA and SiC particles.
- An adhesive and abrasive wear mechanism has been observed in the present study.
- The increase in wear resistance can be attributed to the strengthening mechanism of the matrix which results from the thermal mismatch between the reinforcements and the matrix.
- Mechanical mixing took place between the pin and the counterface disk indicating the greater wear resistance of the composites.

Conflicts of interest

The authors declare no conflicts of interest.

REFERENCES

- [1] Siva Prasad D, Rama Krishna A. Tribological properties of A356.2/RHA composites. *J Mater Sci Technol* 2012;28:367–72.
- [2] Siva Prasad D, Shoba Ch, Ramaniah N. Investigations on mechanical properties of aluminium hybrid composites. *J Mater Res Technol* 2014;3(1):79–85.
- [3] Mandal A, Murthy BS, Chakraborty M. Sliding wear behavior of T6 treated A356-TiB₂ in-situ composites. *Wear* 2009;266:865–72.
- [4] Kök M. Abrasive wear of Al₂O₃ particle reinforced 2024 aluminum alloy composites fabricated by vortex method. *Composites A* 2006;37:457–64.
- [5] Alanemea KK, Akintund IB, Olubamb PA, Adewal TM. Fabrication characteristics and mechanical behaviour of rice husk ash – alumina reinforced Al–Mg–Si alloy matrix hybrid composites. *J Mater Res Technol* 2013;2:60–7.
- [6] Suresha S, Sridhara BK. Wear characteristics of hybrid aluminium matrix composites reinforced with graphite and silicon carbide particulates. *Compos Sci Technol* 2010;70:1652–9.
- [7] Mitrović S, Babić M, Stojanović B, Miloradović N, Pantić M, Džunić D. Tribological potential of hybrid composites based on zinc and aluminum alloys reinforced with SiC and graphite particles. *Tribol Ind* 2012;34:177–85.
- [8] Funatani K, Kurosawa K. Composite coatings improve engines. *Adv Mater Processes* 1994;146:27–9.
- [9] Jha AK, Prasad SV, Upadhyaya GS. Sintered 6061 aluminium alloy–solid lubricant particle composites: sliding wear and mechanisms of lubrication. *Wear* 1989;133:163–72.
- [10] Gibson PR, Clegg AJ, Das AA. Wear of cast Al–Si alloys containing graphite. *Wear* 1984;95:193–8.
- [11] Yang JB, Lin CB, Wang TC, Chub HY. The tribological characteristics of A356.2Al alloy/Gr(p) composites. *Wear* 2004;257:941–52.
- [12] Siva Prasad D, Rama Krishna A. Effect of heat treatment on the damping behavior of A356.2/RHA composites. *Bull Mater Sci* 2012;35:989–95.
- [13] Taya M, Arsenault RJ. Metal matrix composites – thermomechanical behavior. New York, USA: Pergamon Publishers; 1989.